J|A|C|S
COMMUNICATIONS

Published on Web 10/31/2002

Thermal Activation of Molecularly-Wired Gold Nanoparticles on a Substrate as Catalyst

Jin Luo, Vivian W. Jones,† Mathew M. Maye, Li Han, Nancy N. Kariuki, and Chuan-Jian Zhong*

Department of Chemistry, State University of New York at Binghamton, Binghamton, New York 13902

Received August 26, 2002

Nanostructured gold catalysis has attracted increasing interest because of the discovery of unprecedented catalytic activity and specificity of gold at nanometer sizes.[1−4] The idea of using core−shell nanoparticles consisting of metal nanocrystal cores and organic monolayer shells to prepare nanostructured catalysts stems from size controllability, monodispersity, processibility, and aggregation-resistivity.[5−8] The catalytic activity of such materials requires, however, the ability to manipulate the interparticle spatial and surface access properties.[9] This ability is inherently linked to the controllable activation of the core−shell nanostructure or removal or reconstitution of the shell components. Electrochemical activation has recently been demonstrated in our laboratory[10] as such a pathway, which requires, however, the use of a supporting electrolyte. Thermolysis of metal-carboxylate-bridged gold nanoparticles[11] for preparing conductive materials and surfactant-capped Pt/Ru nanoparticles[12] or C-supported $PtRu_5C(CO)_{16}$ [13] for preparing catalysts has recently been demonstrated. However, there is little understanding of how the interparticle spatial and surface properties evolve thermally in a controllable way. In this work, we report novel findings of an atomic force microscopic investigation of the thermal activation of molecularly wired gold nanocrystals as nanostructured catalysts. We studied the electrocatalytic oxidation of methanol, which is of fundamental importance to fuel cell catalysis,[14] as a proof-of-concept system. Our aim is to establish a thermal activation strategy viable for processing nanostructured catalysts via spatially defined core−shell nanoparticle assembly.

Gold nanoparticles of 2-nm core size (1.9 ± 0.7 nm, Au_{2-nm}) capped with decanethiolate (DT) monolayer shell were synthesized using a two-phase method.[5−6] The particles were assembled as a thin film on freshly cleaved mica or polished glassy carbon (GC) substrates (0.5 cm^2) by an exchange-cross-linking-precipitation route using 1,9-nonanedithiolate (NDT) as a linking or wiring agent.[15] Such a film consists of both wiring NDT and capping DT molecules. The thickness was controlled by assembling time and monitored by surface plasmon resonance absorbance and mass loading,[15] which was equivalent to a few monolayers or submonolayer coverages.

In Figure 1, a thermogravimetric analysis (TGA) curve is shown for DT-capped Au_{2-nm} particles. The mass decrease starts at about 140 °C and shows a transition at 225 °C. The overall mass change (25 wt %) is consistent with the expectation based on a model calculation of the percentage of the organic shell (26 wt %).[6] On the basis of the TGA data, we hypothesized two extremes of the nanostructure upon thermal activation near the transition temperature. One involves partially capped nanoparticles with intact core size and interparticle space, and the other, naked nanoparticles with a controllable larger core size. The interaction with the shell-opened

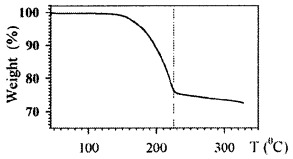

Figure 1. TGA curve of DT/Au_{2-nm} nanoparticles.

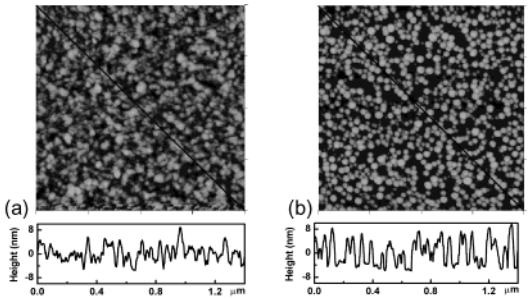

Figure 2. AFM images (1 × 1 μm^2) of ∼2 equivalent layer film of NDT-Au_{2-nm} on mica before (a) and after (b) activation (250 °C) (acquired after cooling to rt). The cross-section view corresponds to the line drawn.

nanocrystals with the substrate surface thus plays an important role in the mobility and the eventual morphology of the nanoparticles. The AFM images described next provided important insights into this hypothesis.

Figure 2 shows a typical set of AFM images for a ∼2 equivalent layer film before and after treatment at 250 °C for 30 min in a muffle furnace. We chose to show the data for a sample with slightly more than one monolayer because the particles are densely packed for comparing the overall morphological changes under the ex situ sampling condition. The particle sizes in the *xy*-plane appear larger than 2 nm, with an apparent overlapping of the outlines of the particles (a). These features are due to a combination of the tip−sample convolution and the tip−shell interaction. The average height of ∼7 nm corresponds to overlapping of about two nanoparticles. After the thermal treatment (b), the outline of individual particles appears much better resolved. The average height for the particles (8.9 ± 2.9 nm) is slightly larger, indicating a small degree of localized aggregation of the overlapped nanoparticles upon the thermal treatment. Similar features were observed for a submonolayer coverage sample. Two sets of spectroscopic data further evidenced the removal of thiolates (Supporting Information). First, infrared reflection spectroscopic analysis showed the absence of the methylene stretching bands. Second, X-ray photoelectron spectroscopic data showed undetectable sulfur species. However, about 8% of oxygen species is detected, which indicates the surface oxidation of gold under the thermal treatment in air.

To precisely compare the morphological evolution under the thermal treatment, particularly at the temperature of ∼225 °C as

* To whom correspondence should be addressed. E-mail: cjzhong@binghamton.edu.
† 3M Corporate Analytical Technology Center, 3M Center, St. Paul, MN 55144-1000.

10.1021/ja028285y CCC: $22.00

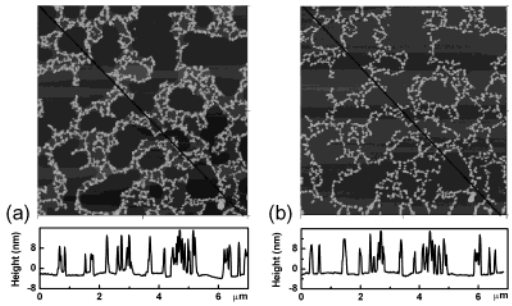

Figure 3. In situ AFM images (5×5 μm^2) of a submonolayer film of NDT-Au_{2-nm} on mica before (a) and after (b) activation (225 °C) (acquired after cooling to rt). Cross-section view corresponds to the line drawn.

indicated in the TGA data, we next carried out in situ AFM imaging by directly mounting the sample on the imaging stage that is coupled to the heating capability. Figure 3 shows a typical set of AFM images for a thin film on mica surface to compare the morphology before and after the thermal treatment at 225 °C for 30 min. We chose to show the data for a sample with a submonolayer because the particles are less densely packed to allow a detailed comparison of the morphological changes by the in situ capability. The particles are clustered into wire- or chainlike morphologies. The cross-section data suggest an overlapping of ~3 nanoparticles in average. The outline of individual nanoparticles is slightly blurred or not well resolved (a). After the treatment (b), not only is the outline of individual particles better resolved, but the chainlike feature also remains intact. The removal of thiolates at this temperature was also supported by the tapping-mode phase imaging data, which reveals that the dark phase contrast (associated with the thiol monolayer) is absent for the thermally treated compared to the as-prepared film (Supporting Information). The height analysis of the cross-section data in Figure 3 reveals 11.1 ± 3.9 nm (a) and 13.1 ± 3.4 nm (b), respectively, suggesting little change in height. The small increase in particle size is believed to be due to localized aggregation largely from the overlapped particles. The unchanged interparticle spatial feature in the *xy*-plane demonstrates that the interparticle spatial property can be controlled even if there is a local aggregation from the overlapped nanoparticles. The combination of the initial molecular wiring and the subsequent adhesive interaction of the particle to the substrate must have played an important role in the spatial fixation. We further note that particles treated at 200 °C revealed a local "melting"-like tendency, in contrast to the feature observed from 250 °C under which the thiolates are removed, suggestive of the propensity of strong particle−substrate interaction and the effect of capping/wiring molecules. These results demonstrate the viability of controlling the interparticle spatial properties by programming the temperature.

The catalytic activity of the activated nanoparticles was examined for the electroxidation of methanol. We note that AFM features of the film on the conductive GC substrate are largely similar to those on mica except for a much rougher morphology due to the substrate effect. In Table 1, we compare the electrocatalytic activity between the thermally activated gold catalysts with the electrochemically activated catalysts based on voltammetric data. The electrocatalytic activity, as recently reported for electrochemically activated catalyst,[10] is characterized by a large anodic wave at $E_{pa} = +250$ mV appearing after applying a positive potential (+800 mV). In comparison, the anodic current density (i_{pa}) for the thermally activated film is twice as large as the electrochemically activated catalyst (same film thickness), with the oxidation potential being slightly less positive than the electrochemically activated film. A

Table 1. Electrocatalytic Properties for Activated NDT-Au_{2-nm} Film (~5 Layers) on GC in 0.5 M KOH + 3 M Methanol (from CV data at 50 mV/s)

	electrooxidation of methanol	
activation treatment	i_{pa} (μA/cm^2)	E_{pa} (mV vs SCE)
thermal	166	+250
electrochemical	82	+270

closer examination reveals two overlapping anodic waves at 220 and 300 mV, indicating the existence of at least two different catalytic sites for the thermally activated catalysts. The results thus demonstrate that the nanostructured catalytic activity can be thermally activated by the controlled temperature.

In conclusion, we have demonstrated that the molecularly wired nanoparticles can be thermally activated by manipulating temperature to produce nanoparticle catalysts with controllable size and largely intact interparticle morphology. We further note that dependencies of the interparticle morphology on temperature, wiring structure, and substrate are also reflected by an evolution of the surface plasmon resonance band of the nanoparticles (see Supporting Information). These findings have important implications to the design of nanostructured catalysts via molecular wiring. We are currently investigating different molecular structures of the wiring agents and are developing an in-depth correlation of the structural evolution in particle size and interparticle spatial and substrate surface properties.

Acknowledgment. Financial support of this work from the ACS-PRF and 3M Corporation is gratefully acknowledged.

Supporting Information Available: Additional data (AFM, IRS, XPS, UV−vis) (PDF). This material is available free of charge via the Internet at http://pubs.acs.org.

References

(1) Haruta, M. *Catal. Today* **1997**, *36*, 153.
(2) Valden, M.; Lai, X.; Goodman, D. W. *Science* **1998**, *281*, 1647.
(3) (a) Sanchez, A.; Abbet, S.; Heiz, U.; Schneider, W. D.; Hakkinen, H.; Barnett, R. N.; Landman, U. *J. Phys. Chem. A* **1999**, *103*, 9573. (b) Heiz, U.; Sanchez, A.; Abbet, S.; Schneider, W. D. *Chem. Phys.* **2000**, *262*, 189. (c) Schmid, G.; Emde, S.; Maihack, V.; Meyer-Zaika, W.; Peschel, S. *J. Mol. Catal. A: Chem.* **1996**, *107*, 95.
(4) Bond, G. C.; Thompson, D. T. *Gold Bulletin* **2000**, *33*, 41.
(5) Brust, M.; Walker, M.; Bethell, D.; Schiffrin, D. J.; Whyman, R. *J. Chem. Soc., Chem. Commun*. **1994**, 801.
(6) (a) Hostetler, M. J.; Wingate, J. E.; Zhong, C. J.; Harris, J. E.; Vachet, R. W.; Clark, M. R.; Londono, J. D.; Green, S. J.; Stokes, J. J.; Wignall, G. D.; Glish, G. L.; Porter, M. D.; Evans, N. D.; Murray, R. W. *Langmuir* **1998**, *14*, 17. (b) Hostetler, M. J.; Zhong, C. J.; Yen, B. K. H.; Anderegg, J.; Gross, S. M.; Evans, N. D.; Porter, M. D.; Murray, R. W. *J. Am. Chem. Soc.* **1998**, *120*, 9396. (c) Shon, Y. S.; Gross, S. M.; Dawson, B.; Porter, M.; Murray, R. W. *Langmuir* **2000**, *16*, 6555.
(7) Maye, M. M.; Zheng, W. X.; Leibowitz, F. L.; Ly, N. K.; Zhong, C. J. *Langmuir* **2000**, *16*, 490.
(8) Templeton, A. C.; Wuelfing, W. P.; Murray, R. W. *Acc. Chem. Res*. **2000**, *33*, 27 and references therein.
(9) Zhong, C. J.; Maye, M. M. *Adv. Mater.* **2001**, *13*, 1507.
(10) (a) Maye, M. M.; Lou, Y. B.; Zhong, C. J. *Langmuir* **2000**, *16*, 7520. (b) Lou, Y. B.; Maye, M. M.; Han, L.; Luo, J.; Zhong, C. J. *Chem. Commun.* **2001**, 473. (c) Luo, J.; Lou, Y. B.; Maye, M. M.; Zhong, C. J.; Hepel, M. *Electrochem. Commun.* **2001**, *3*, 172.
(11) Wuelfing, W. P.; Zamborini, F. P.; Templeton, A. C.; Wen, X. G.; Yoon, H.; Murray, R. W. *Chem. Mater.* **2001**, *13*, 87.
(12) Paulus, U. A.; Endruschat, U.; Feldmeyer, G. J.; Schmidt, T. J.; Bonnemann, H.; Behm, R. J. *J. Catal.* **2000**, *195*, 383.
(13) Nashner, M. S.; Frenkel, A. I.; Somerville, D.; Hills, C. W.; Shapley, J. R.; Nuzzo, R. G. *J. Am. Chem. Soc.* **1998**, *120*, 8093.
(14) Acres, G. J. K.; Frost, J. C.; Hards, G. A.; Potter, R. J.; Ralph, T. R.; Thompsett, D.; Burstein, G. T.; Hutchings, G. J. *Catal. Today* **1997**, *38*, 393.
(15) (a) Leibowitz, F. L.; Zheng, W. X.; Maye, M. M.; Zhong, C. J. *Anal. Chem*. **1999**, *71*, 5076. (b) Zheng, W. X.; Maye, M. M.; Leibowitz, F. L.; Zhong, C. J. *Anal. Chem*. **2000**, *72*, 2190.

JA028285Y